Rapid, high-throughput phenotypic profiling of endosymbiotic dinoflagellates (Symbiodiniaceae) using benchtop flow cytometry

Colin J. Anthony*, Colin Lock, Bastian Bentlage†

Marine Laboratory, University of Guam, Mangilao, Guam, United States

* colin_anthonynw@outlook.com

† bentlageb@triton.uog.edu

Short title: Flow cytometric phenotypic profiling of Symbiodiniaceae

Keywords: method, phenotype, autofluorescence, symbiosis, coral

Abstract

Endosymbiotic dinoflagellates (Family Symbiodiniaceae) are the primary producer of energy for many cnidarians, including corals. The intricate coral-dinoflagellate symbiotic relationship is becoming increasingly important under climate change, as its breakdown leads to mass coral bleaching and often mortality. Despite methodological progress, assessing the phenotypic traits of Symbiodiniaceae *in-hospite* remains a complex task. Bio-optics, biochemistry, or "-omics" techniques are expensive, often inaccessible to investigators, or lack the resolution required to understand single-cell phenotypic states within endosymbiotic dinoflagellate assemblages. To help address this issue, we developed a protocol that collects information on cell autofluorescence, shape, and size to simultaneously generate phenotypic profiles for thousands of Symbiodiniaceae cells, thus revealing phenotypic variance of the Symbiodiniaceae assemblage to the resolution of single cells. As flow cytometry is adopted as a robust and efficient method for cell counting, integration of our protocol into existing workflows allows researchers to acquire a new level of resolution for studies examining the acclimation and adaptation strategies of Symbiodiniaceae assemblages.

1. Introduction

Symbiodiniaceae are dinoflagellates known for their endosymbiotic relationship with many marine invertebrates, most notably reef building corals [1]. The breakdown of this symbiosis can lead to coral bleaching and mortality [2]. Despite methodological progress identifying functional and genetic variation in Symbiodiniaceae, assessing trait variation of Symbiodiniaceae *in-hospite* remains a complex task [3]. Pulse Amplitude Modulated (PAM) fluorometry is widely used to quantify photosynthetic efficiency of Symbiodiniaceae photosystems *in-hospite* [4] both *in situ* [5] and *ex situ* [6]. However, PAM fluorometry provides an aggregate measure of photosystem performance for the Symbiodiniaceae population and does not quantify variation in photosystem performance between cells within the symbiont population. Isolation, characterization, and quantification of photopigments using spectrometry or fluorometry struggles with similar resolution issues, relying on the extraction of pigments from cells prior to analysis, followed by the normalization of measured pigment quantities to observed cell densities or overall protein content [7]. Microscopic methodologies are capable of quantifying phenotypic differences of single Symbiodiniaceae cells, but these methodologies are labor intensive, able to process only a small number of cells, and often require multiple preparation methods or instruments to collect different phenotypic traits [8,9]. By contrast, flow cytometry is a rapid method to quantify phenotypic variation within a Symbiodiniaceae population [10–12] by generating thousands of phenotypic profiles simultaneously and requiring comparatively little sample preparation time. Phenotypic profiles generated by flow cytometry include metrics associated with cell shape, cell size, and photopigments. Flow cytometry is commonly used to count Symbiodiniaceae cells [13], but the additional phenotypic data recorded by the instrument has thus far been largely ignored in Symbiodiniaceae research. To facilitate the use of these data, we provide a detailed protocol and

conducted sensitivity analyses to provide guidance for sample preparation for flow cytometric phenotypic profiling of Symbiodiniaceae.

Flow cytometry was developed in 1968 [14] and has experienced massive advances in the last 50 years moving from a method for cell counting to detecting fluorescent protein markers, detecting RNA expression, describing cell cycles by staining DNA, studying signal pathways with antibodies, sorting cells, and quantifying protein content with fluorescent tags [15]. In the early 1980s, several groups began to highlight the power of flow cytometry for phytoplankton research, demonstrating its ability to characterize phytoplankton communities' taxonomic composition using photopigment autofluorescence, cell size, and cell shape [16,17]. Flow cytometry has also been employed for the rapid quantification of autofluorescent photopigments by measuring the relative strength of their fluorescent signals [10,11,17–23]. Within coral biology, flow cytometry is widely used for determining Symbiodiniaceae cell density [13], but has also been used to identify functional groups and phenotypes of Symbiodiniaceae [10,24], quantify autofluorescent pigments [11,18,19], enumerate endosymbiotic bacterial communities [25,26], and even examine cell cycle dynamics [27–29]. Built from these concepts and methodologies, we developed a straight-forward flow cytometry protocol that generates consistent phenotypic profiles for thousands of individual Symbiodiniaceae cells to quantify the phenotypic variation of the entire assemblage, a currently difficult to access level of resolution. Sample degradation may influence the metrics collected by our protocol and we provide recommendations for sample preparation and handling based on sensitivity analyses conducted by us. Our protocol has the potential to reveal phenotypic differences between Symbiodiniaceae communities and may help elucidate whether phenotypic variation in Symbiodiniaceae assemblages is caused by phenotypic plasticity of Symbiodiniaceae cells or changes in community composition (e.g. shuffling to new functionally advantageous

lineages). With proper implementation and considerations of methodological limitations, the protocol described here can be used to expediently identify functional differences in Symbiodiniaceae assemblages between host species, sampling sites, timepoints, and potentially phenotypic variation and niche partitioning of Symbiodiniaceae communities within a single host.

2. Materials and Methods

2.1 Protocol

The protocol described in this article identifies Symbiodiniaceae cells based on their high red autofluorescence (Fig 1A), and then uses forward scatter, side scatter, red fluorescence, and green fluorescence to generate phenotypic profiles for individual Symbiodiniaceae cells from an endosymbiotic assemblage. The protocol was developed using the Guava easyCyte 6HT-2L (Luminex Corporation, Austin, TX) benchtop flow cytometer and is publicly available through protocols.io (https://www.protocols.io/private/4DD4507110B911EE9A3E0A58A9FEAC02 (doi will be released prior to publication)).

2.2 Identifying signals of autofluorescence

Our flow cytometry protocol relies on the detection of autofluorescence through the excitation of Symbiodiniaceae cells with a blue (488 nm) laser and emission detectors in the green (525/30 nm) and red (695/50 nm) spectra, termed green fluorescence and red fluorescence, respectively (Fig 1B-C).

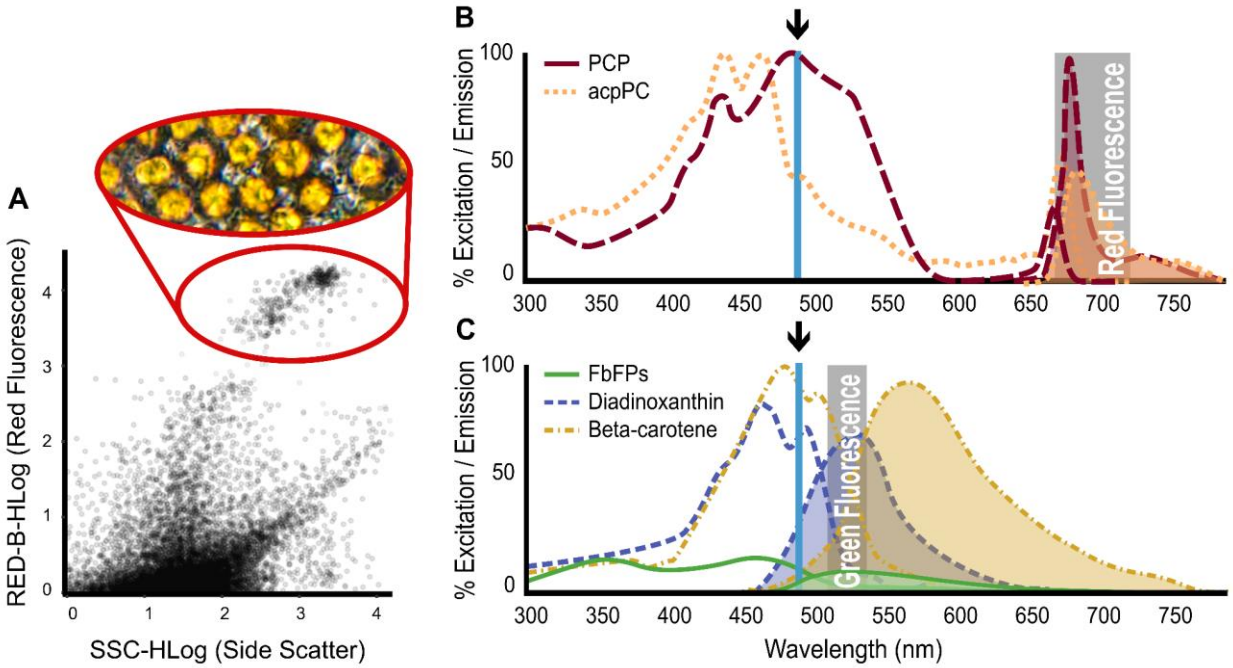

Fig 1. A) Sample point cloud visualizing all cytometry-detected particles within a well-replicate, and demonstrating how Symbiodiniaceae cells are identified based on high red fluorescence (**red circle**). **B-C**) Excitation/emission spectra employed by the flow cytometry protocol presented in this contribution. Excitation laser wavelengths are indicated by arrows. Lines depict absorption spectra, while lines with shaded areas underneath illustrate the intensity of emission wavelengths based on the corresponding excitation laser. **B**) The blue laser (488 nm) simultaneously excites the two dominant light harvesting complexes (LHC) of Symbiodiniaceae (PCP and acpPC) and a set of antioxidant associated pigments: FbFPs, diadinoxanthin, and beta-carotene (**C**). The two groups fluoresce differently upon excitation, which are differentiated with two emission filters that detect red (695/50 nm) (**B**) and green (525/30 nm) (**C**) spectra (**grey boxes**).

In other flow cytometry methods, researchers typically compensate for spillover and spectral overlap by using labeled antibodies as controls to compensate for cellular autofluorescence and other contaminating fluorophores. This makes sense when using flow

cytometry to detect labeled cellular structures (e.g. induction of labeled proteins through heat shock), but the quantification of autofluorescence requires different techniques given the high protein diversity and spectral overlap within an excitation-emission profile [23]. By identifying all possible targets within Symbiodiniaceae [7,30–32] and modeling their excitation and emission profile based on previously published literature [33–38], we can infer sources of autofluorescence.

Excitable pigments previously identified from Symbiodiniaceae include beta-carotene, chlorophyll *a*, chlorophyll c_2, diadinoxanthin, diatoxanthin, and peridinin [7,31]. We also identified flavin-based fluorescent proteins (FbFPs) as a probable source of autofluorescence [30,39,40]. To model our autofluorescence targets and identify any risk of spectral overlap, spectral properties of the peridinin-chlorophyll *a* light-harvesting antennae protein complex (PCP) and riboflavin (FbFPs), compensated for blue (488 nm) laser excitation, were visualized using FluoroFinder Spectra Viewer (https://app.fluorofinder.com/ffsv/svs/). Beta-carotene [34], diadinoxanthin [37] and the chlorophyll *a*-chlorophyll c_2-peridinin protein complex (acpPC) [38] spectra were mapped and normalized to each other using the FluoroFinder spectra and absorbance spectra from Bricaud et al. [41].

2.3 Optimization assays. Photopigments are labile molecules prone to degradation in ambient conditions [42], as are Symbiodiniaceae cells when prepared improperly (see Sections 3.2 and 3.3). Two simple assays were designed and performed to provide a framework for optimizing the protocol. In both optimization assays, ideal conditions (temperature, dilution, time, etc.) were selected based on distributions with the highest consistency and tightest variances. This included FSC (forward scatter representing cell size) and SSC (side scatter representing cell shape), which are not only valuable phenotypic traits, but can also be used to detect potential cell clumping and cell lysing, respectively [43–46].

(1) Assay one was used to determine the impacts of time, temperature, and light conditions on samples and the resulting data. A single staghorn coral (*Acropora pulchra*) fragment was airbrushed with filtered, sterile seawater to create a 30 mL (~150,000 cells/mL) tissue slurry. The slurry was homogenized by vortexing and needle shearing (S1 File), then equally distributed across four 50 mL falcon tubes. One mL of the tissue slurry was aliquoted from each falcon tube and immediately processed using our flow cytometry protocol (S1 File). After aliquots were removed, falcon tubes were separated and exposed to one of four conditions: (1) dark on ice, (2) dark at room temperature (22°C), (3) ambient light on ice, and (4) ambient light at room temperature. A 1 mL sample from each falcon tube was processed approximately every two hours for a total of eight hours; a final set of samples was processed after being stored in their respective conditions overnight. This yielded six temporal samples processed 43, 136, 236, 344, 470, and 1459 minutes after removing tissue from the skeleton. At each time point, treatment replicates were loaded across three wells, and each well was sampled by the flow cytometer twice, creating six technical replicates per sample. Pairwise Dunn's tests (Z) were calculated using the FSA R package v0.9.3 [47], then organized into a compact letter display using the cldList command from the rcompanion package v2.4.21 [48]

(2) Assay two was used to optimize tissue slurry dilutions and to identify possible effects of flow cytometer run times. We prepared six 1 mL (~150,000 cells/mL) tissue slurries from a single *Acropora pulchra* fragment for flow cytometry using our protocol (S1 File). Before loading samples into a 96-well microwell plate, all processed tissue slurries were combined into a single 50 mL falcon tube, needle sheared, and vortexed to homogenize samples to avoid possible batch effects. 50x, 20x, 10x, 5x, 2x, and 1x dilutions of the combined tissue slurry were prepared directly in the 200 uL wells. This created a total of 16 dilution series replicates, processed in sequential

order until all 96 wells of the plate were filled. The flow cytometer processed each replicate dilution (2 within well technical replicates) at ~5 min intervals leading to breaks of 30-40 minutes between wells of the same dilution. until the run was complete. Time between replicates and dilutions are approximate as sample acquisition varies depending on the concentration of the sample.

2.4 Example Application. In addition to the optimization assays, we performed an acclimation experiment with the upside-down jellyfish *Cassiopea*, a model organism often used to better understand bleaching and symbiosis [49], to demonstrate data handling techniques and discuss data interpretation. Clonal *Cassiopea* were placed into three different conditions for three weeks each. Clonal *Cassiopea* were obtained from UnderWater World Aquarium in Tumon, Guam. *Cassiopea* were transferred to flow through tanks at the University of Guam Marine Laboratory in Mangilao Guam on April 1, 2022 and allowed to acclimate until the start of the experiment on June 8, 2022. Jellyfish were 55-79 mm in diameter at the start of the experiment. Group 1 (n=4) was placed in low-light conditions (50% shade), group 2 in high-light conditions (no shade) (n=4), and group 3 experienced variable light conditions (n=5) rotating from high-light to low-light to high-light (one week per condition). At the end of three weeks, digitate cirri (clusters of tentacle-like structures attached to the top of each oral arm) [50] were sampled with sterile scissors from each individual and placed in 1 mL of filtered seawater. Symbiodiniaceae cells were subsequently extracted and processed following the flow cytometry protocol described here (S1 File).

After identifying the Symbiodiniaceae cells based on red autofluorescence (Fig 1A), particulate noise was removed from the dataset (RED-B-HLog < 3.04001) yielding sample sizes of 16,134, 18,464, and 19,821 single-cell Symbiodiniaceae fluorescent profiles for dark, light, and variable treatment groups, respectively. To better understand data structure, power, and effect size,

the effect of experimental conditions was analyzed at two resolutions: (1) phenotypic profiles of Symbiodiniacaeae within each condition visualized and analyzed as entire assemblages, independent of host (n=16,134, 18,464, 19,821) and (2) Symbiodiniaceae assemblages averaged to their respective host jellyfishes before visualizing and analyzing the effect of treatments (n = 4, 4, 5). A principal component analysis was performed and results plotted using the base stats package in R [51] to visualize the phenotypic variation associated with each experimental group. At both resolutions treatment groups were compared by using non-parametric Kruskal-Wallis tests (X^2) followed by post-hoc pairwise Dunn's tests (Z) using the FSA R package v0.9.3 [47]. All data processing and analysis for both of the optimization assays and the example application was completed with R v4.1.2 [51] in RStudio v1.3.1073 [52]. Figures were generated and modified with a combination of ggplot2 v3.3.5 [53] and InkScape v1.1 (https://inkscape.org).

All code and datasets required to replicate optimization assay and example application experiment analyses have been deposited on a public GitHub repository (https://github.com/AnthonyCuog/CytometryProtocol (doi will be released prior to publication)).

3. Results

3.1 Fluorescent pigment identification. Red light emission caused by excitation with a blue laser is most likely caused by the core light harvesting complexes (LHC), peridinin-chlorophyll *a* light-harvesting antennae protein complex (PCP) or the chlorophyll a-chlorophyll c2-peridinin protein complex (acpPC) (Fig 1B), which use peridinin as the primary light harvesting molecule before efficiently passing it to chlorophylls [54]. This is in agreement with current literature that links red fluorescence off a 488 nm laser to chlorophyll [10,11,18,19]. However, we suggest that due to chlorophylls intrinsic association with peridinin in Symbiodiniaceae [38,55], we suggest

identifying this fluorescence signature as LHCs or LHC-associated photopigments as it is more conservative and accurate for Symbiodiniaceae.

Increased green fluorescence in dinoflagellates under stress has been attributed to beta-carotene [11]. However, diadinoxanthin, diatoxanthin [37,56], and flavin-based fluorescent proteins (FbFPs) [30,39,40] also emit green fluorescent light when excited by blue light (Fig 1C). We interpret green fluorescence as the combined signature of beta-carotene, xanthophylls (diadinoxanthin and diatoxanthin), and flavins given their fluorescent spectral overlap (Fig 1C).

3.2 Effects of sample preparation on degradation. Samples stored on ice and processed within approximately two hours (136 minutes) showed the most consistent signatures across all measurements (Fig 2). Red fluorescence degraded across all groups, but remained the most stable in the dark on ice, specifically for samples prepared within the first two time points (136 minutes) (Fig 2A). Green fluorescence (Fig 2B), forward scatter (Fig 2C), and side scatter (Fig 2D) were relatively stable compared to red fluorescence, although slightly higher readings in side scatter could indicate some cell lysing after prolonged preparation times (Fig 2D). Cell concentrations were consistent across all treatments when processed within 136 minutes (Fig 2E).

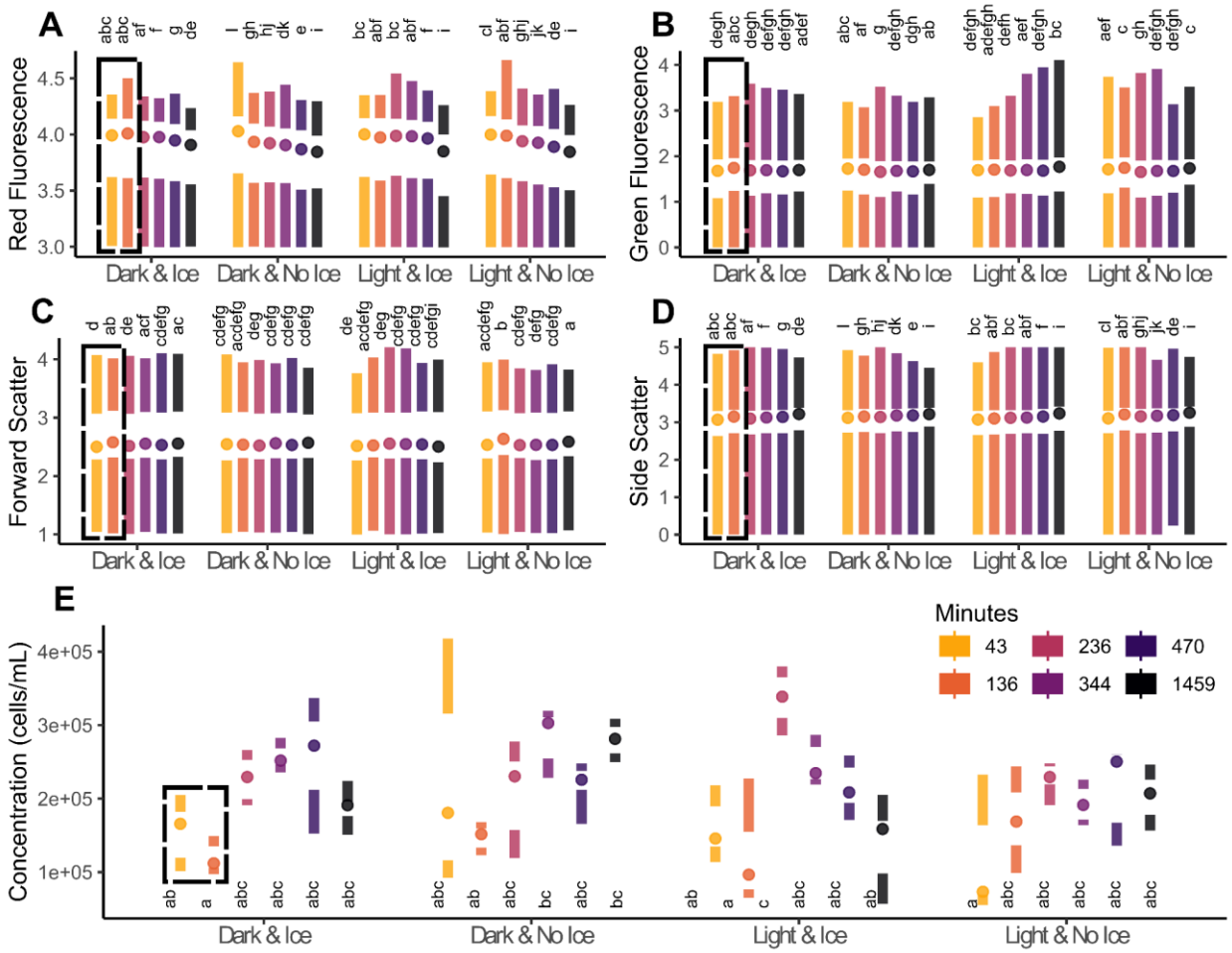

Fig 2. Samples prepared under different light (Dark vs Light) and temperature (Ice vs No Ice) conditions. Samples processed on ice within roughly two hours (136 minutes) of airbrushing yielded the most consistent results (**dashed boxes**), as informed by the statistical groups ($p < 0.05$) that are represented by letters **A**) Red fluorescence degraded quickly. **B**) Green fluorescence and forward scatter (cell size) (**C**) remained relatively stable over time. **D**) Side scatter (cell roughness), increased with time **E**) Cell concentrations were relatively consistent results when processed within 136 minutes.

3.3 Effects of dilution and flow cytometer run-time on degradation. Six dilutions (50x, 20x, 10x, 5x, 2x, and 1x) were tested 16 times each across a 96-well plate resulting in individual sample

measurements of ~150,000 cells/mL for each replicate (Fig 3). The flow cytometer run took around six hours to complete. Ten-fold and five-fold dilutions in the first four rows of the 96-well plate were the most consistent. More diluted samples produced unstable means of measured parameters, while less diluted samples exacerbated degradation. Red fluorescence decreased with time (Fig 3A), while green fluorescence increased with time (Fig 3B). Cell size (forward scatter) remained relatively consistent, but forward scatter increased in highly concentrated samples, overestimating cell size likely due to cell clumping (Fig 3C). Cell shape (side scatter) was the most stable metric suggesting low rates of cell lysis, though increasing quartile ranges in the one-fold and two-fold dilutions suggested increased susceptibility to lysis in higher concentrations (Fig 3D). Estimates of cell concentrations were heavily affected by dilution and run-time (Fig 3E).

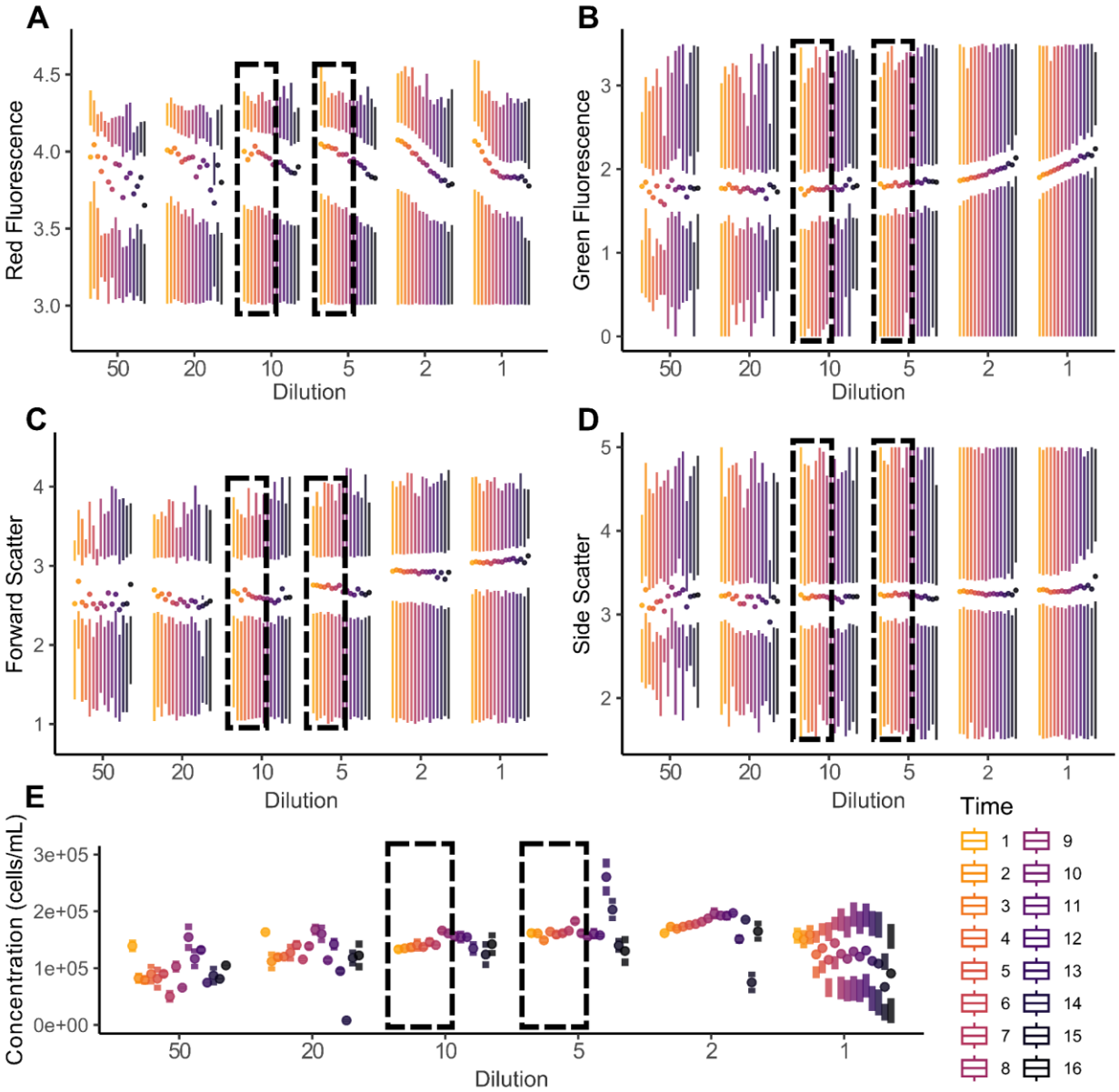

Fig 3. Six dilutions (50x, 20x, 10x, 5x, 2x, and 1x) were tested 16 times each across a 96-well plate. The cytometry run took ~6 hours estimating ~20 minutes between each of the 16 replicates (**Time**). Ten-fold and five-fold dilutions were the most consistent for half of the plate (**dashed boxes**) suggesting that runs should be limited to ≤ 48 wells (half of a standard 96-well plate). Over- or under-dilution of samples had a large effect on resulting parameter estimates. **A**) Red fluorescence degraded over time and had more variation with 50x and 20x dilutions. **B)** Green

fluorescence increased over time, presumably due to heat generated by the flow cytometer. **C**) Cell size (FSC) did not change over time, but highly concentrated samples led to an overestimation of cell sizes, likely due to cell clumping. **D**) Cell shape (SSC) was the most stable parameter, suggesting low rates of cell lysis. **E**) Cell concentrations were heavily affected by dilution and time spent in the flow cytometer.

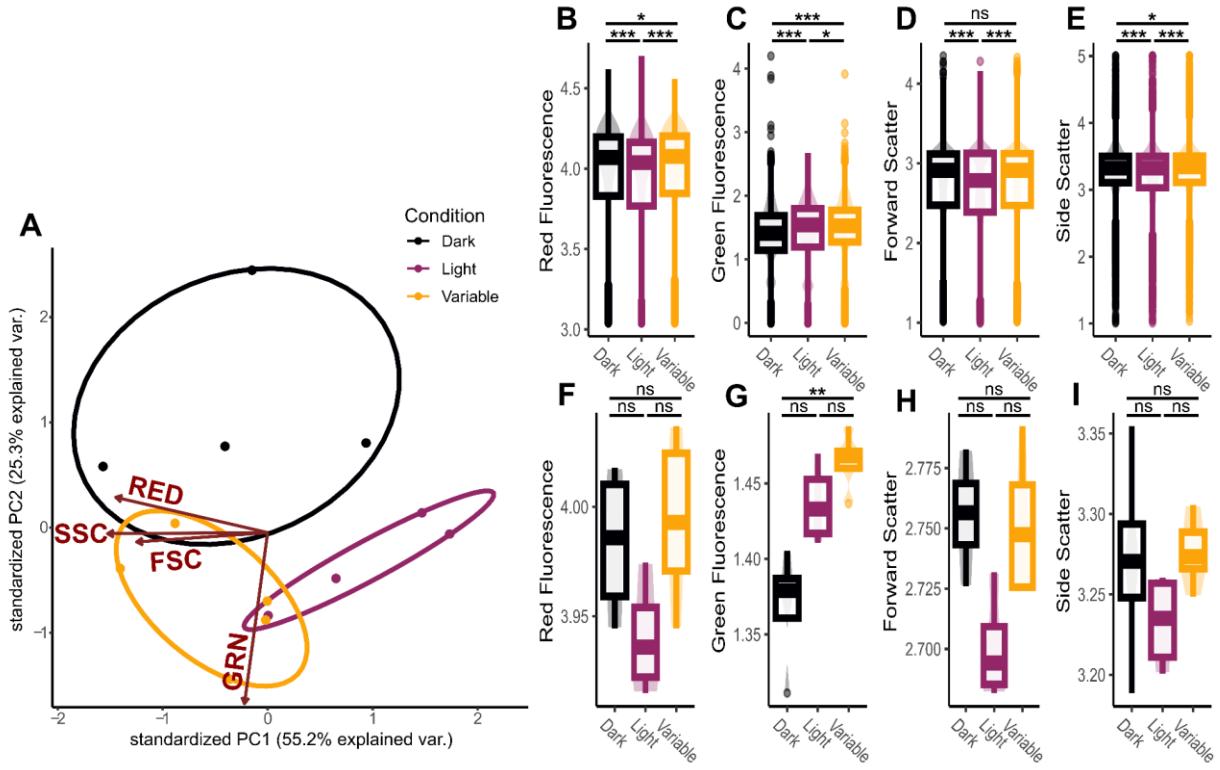

Fig 4. Phenotypic profiles built from red fluorescence, green fluorescence, forward scatter, and side scatter for upside-down jellyfish processed with our flow cytometry protocol (S1 File) after three weeks of exposure to different light conditions (Dark, Light, and Variable). **A**) Principal component analysis demonstrating divergence of phenotypic profiles associated with jellyfish of different experimental light conditions. **B-I**) Distributions for each phenotypic trait used to

generate a phenotypic profile. Lines with asterisk indicate pairwise comparisons tested with Post-Hoc Dunn's tests ranging producing three categories for p-values: $p > 0.05$ (ns), $p < 0.05$ (*), and $p < 0.001$ (***). **B-E**) Each distribution represents 16,000 - 20,000 observations, representing the true phenotypic variance within a Symbiodiniaceae assemblage, which allowed for discriminating between treatments, even with small effect size. **F-I**) Phenotypic measurements averaged to the jellyfish host to better resolve conditional effect, despite decreased statistical power.

3.4 Upside-down jellyfish light acclimation experiment. After three weeks, *Cassiopea* medusae visibly changed color with dark-acclimated individuals being dark brown and light-acclimated individuals being light brown. Alongside a visible change in medusa color, PCA indicated a substantial phenotypic shift within the Symbiodiniaceae assemblage, especially between the light and dark acclimated individuals, while the variable light exposure group showed a more mixed signal (Fig 4A). Treatment influenced fluorescence readings for all excitation/emission parameters, but statistical power varied depending on whether phenotypic variation was compared at the level of individual Symbiodiniaceae cells (Fig 4B-E) or at the level of mean phenotypic variance within each host (Fig 4F-I). Light-acclimated individuals had the lowest red fluorescence (LHC photopigments), forward scatter (cell size), and side scatter (cell shape), while dark-acclimated individuals had the lowest green fluorescence signal ('antioxidant' pigments) (Fig 4B-I). When all Symbiodiniaceae measurements were included and compared across treatments (Fig 4B-E), Dunn's tests identified statistically significant differences ($p < 0.001$) in most pairwise comparisons of treatments, despite small effect sizes. When averaging phenotypic variance to the jellyfish host individuals ($n = 4$ or 5), statistics were less powerful, but treatment effects became more conspicuous (Fig 4F-I).

4. Discussion

4.1 Symbiodiniaceae fluorescence, light scatter, and phenotype. The purpose of the described methodology is to rapidly generate a phenotypic profile for thousands of individual Symbiodiniaceae cells, not necessarily to identify underlying mechanisms of phenotypic acclimation (e.g. photopigment regulation), although there is a substantial body of literature that uses flow cytometry to directly quantify chlorophyll or other pigments [10,11,17,19,21,22,57,58]. In our example experiment (Fig 4), we revealed differences in Symbiodiniaceae phenotypes associated with different light conditions (Fig 4A). Symbiodiniaceae do not possess chlorophyll *b* *[7,31]*, a chlorophyll molecule common in other photosynthetic organisms that would normally be detected by our excitation-emission profiles. Instead, Symbiodinaceae possess two major LHC antennae, the peridinin-chlorophyll *a* protein complex (PCP) and the chlorophyll *a*-chlorophyll c_2-peridinin protein complex (acpPC), which use peridinin and chl c_2 as the primary light-harvesting pigments [54,59,60]. Understanding Symbiodiniaceae-specific photosynthetic structures may influence flow cytometry data interpretation and inferences of phenotypic differences. For example, based on our modeled excitation/emission spectra, red fluorescence most likely reflects the relative quantity of LHC antennae or associated light harvesting pigments, primarily peridinin (Fig 1B). This is consistent with other studies that refer to this excitation/emission signature as chlorophyll [11,17–19,58], using flow cytometry for direct quantification of relative pigment abundance [10,21,22]. Our review of Symbiodiniaceae LHC composition and subsequent spectral mapping indicates that red fluorescence is likely targeting peridinin within peridinin-chlorophyll protein complexes (Fig 1A). While red fluorescence may indicate relative pigment abundance, it is possible that changes in red fluorescence are caused by changes in chloroplast size or location [61]. The tight association of peridinin with chlorophylls in LHC antennae [35,54,59,60,62,63] and the extensive literature using flow cytometry to quantify chlorophyll or other pigments

[10,11,17,19,21,22,57,58] supports an interpretation of the reorganization of LHC protein complexes and their associated photopigments. For example, a conservative interpretation of red fluorescence in our *Cassiopea* acclimation experiment (Fig 4) is as follows: 'The reduction in the intensity of red fluorescence in high light could indicate the downregulation of photosynthetic pigments within Symbiodiniaceae cells to reduce light-associated stress'. This interpretation is consistent with the down regulation of PCP that has been associated with light and heat stress [64].

Other studies that have measured green autofluorescence with flow cytometry identified it as beta-carotene [11,23,65]. However, after reviewing the available literature [7,30,34,37,38], we suggest that the intensity of green fluorescence represents a combination of photo-protective and antioxidant pigments and proteins that play primary roles in photo-acclimation and stress mitigation (Fig 1B). Beta-carotene is an efficient reactive oxygen species (ROS) scavenger, especially in the vicinity of high concentrations of ROS [66–68]. Diadinoxanthin and diatoxanthin are the main components in the photoprotective xanthophyll cycle, dissipating excess energy through non-photosynthetic quenching [56], alongside production of antioxidants [69]. The most abundant FbFPs (cryptochromes and riboflavin) act as key stress regulators [70,71] and induce the accumulation of antioxidants [72–74]. Perhaps the relatively high intensity of green fluorescence in high light and variable light jellyfish individuals indicates the upregulation of antioxidant associated photopigments within Symbiodiniaceae cells to reduce light-associated stress (Fig 4).

The protocol presented here targets key LHC pigments (red fluorescence) and a combination of proteins known for their role in photo-acclimation and stress mitigation (green fluorescence) (Fig 1C) in conjunction with well-established measurements reflective of cell size (forward scatter) and cell shape (side scatter) [43,44,46,75] to generate phenotypic profiles of

Symbiodiniaceae. Independent of the underlying pigments, cell size, or cell shape, readings from the flow cytometer reflect phenotypes of individual cells, which may be influenced by the state of the cell (e.g. its progression through the reproductive cell cycle [29]). Large sample sizes, as generated by flow cytometry, enable the estimation of the average phenotypic profile within a Symbiodiniaceae assemblage. The protocol presented here represents a rapid method for high-throughput phenotypic profiling of Symbiodiniaceae assemblages, allowing for the estimation of phenotypic variance of Symbioodiniaceae communities and identification of average phenotypic difference across Symbiodiniaceae assemblages sampled from different hosts or experimental conditions (Fig 4), filling a gap in existing methodologies.

4.2 Protocol performance and optimization.

Photopigments are labile molecules prone to degradation in ambient conditions [42], as is cell morphology when prepared improperly (Figs 2,3). Therefore, it is important to work consistently and expediently. This includes maintaining a consistent processing environment, sample concentrations and quantities, sample preservation methods, gain settings and calibration of the flow cytometer. Samples processed at room temperature were prone to rapid degradation, yielding imprecise estimates of fluorescent parameters compared to consistent autofluorescence-based phenotypic profiles for samples stored and processed on ice (Fig 2). However, autofluorescence signatures still changed after tissue removal from coral skeletons when processing was delayed, even when stored on ice. Based on our observations (Fig 2), we recommend that samples are processed for flow-cytometry within two hours of beginning sample preparation.

Cell concentration and flow-cytometer run-time are further factors to consider. Based on our assay (Fig 2), 5-fold to 10-fold dilutions of a sample with a starting concentration of ~150,000

cells/mL produced the most consistent dataset (15,000 – 30,00 cells/mL) (Fig 3). Over-dilution led to variable means and high variances of fluorescent parameters, while under-dilution exacerbated degradation and may have caused cell clumping, as indicated by increasing forward and side scatters (Fig 3). Independent of concentration, samples began to degrade after processing four rows (48 wells) of the 96-well plate (Fig 3). Therefore, we recommend loading no more than half of a 96-well plate per run with each well containing an estimated concentration of 15,000-30,000 cells/mL. None of the observed patterns were caused by settled cells, as each replicate was vortexed before being loaded into a microwell, and the flow cytometer automatically stirred each sample at a high velocity for seven seconds before data acquisition. The analyses presented here provide a roadmap for implementing and optimizing our flow-cytometry protocol. We recommend investing protocol optimization time upfront. Once established, our protocol should work across a diverse set of hosts, including corals, jellyfish, and hydroids, requiring little ongoing maintenance or cost.

Our *Cassiopea* acclimation experiment represents an example application of our protocol for comparisons of Symbiodiniaceae assemblages originating from different host individuals (Fig 4). The ability to detect extremely small, yet statistically significant effect sizes is a strength of flow cytometry, as it enables the rapid collection of large sample sizes. Large sample sizes increase statistical power, explaining why Symbiodiniaceae traits were statistically different across treatments despite seemingly small effect sizes when comparing measurements of Symbiodiniaceae cells directly between treatments (Fig 4A-C). When averaging measurements from Symbiodiniaceae by host individuals, trends were more conspicuous but statistical power of our treatment comparisons weakened due to the low sample size of 4-5 host individuals per treatment (Fig 4D-F). Both levels of resolution are informative, but resolution of single

Symbiodiniaceae cells is a more accurate representation of population-level phenotypic variance and provides greater statistical power for comparisons. We recommend researchers consider effect size and statistical power given their factorial resolution. The integration of the protocol presented here alongside other commonly used methodologies (e.g. PAM fluorometry, transcriptomics, or ITS2 metabarcoding) may help provide a more complete picture of Symbiodiniaceae acclimation and adaptation dynamics.

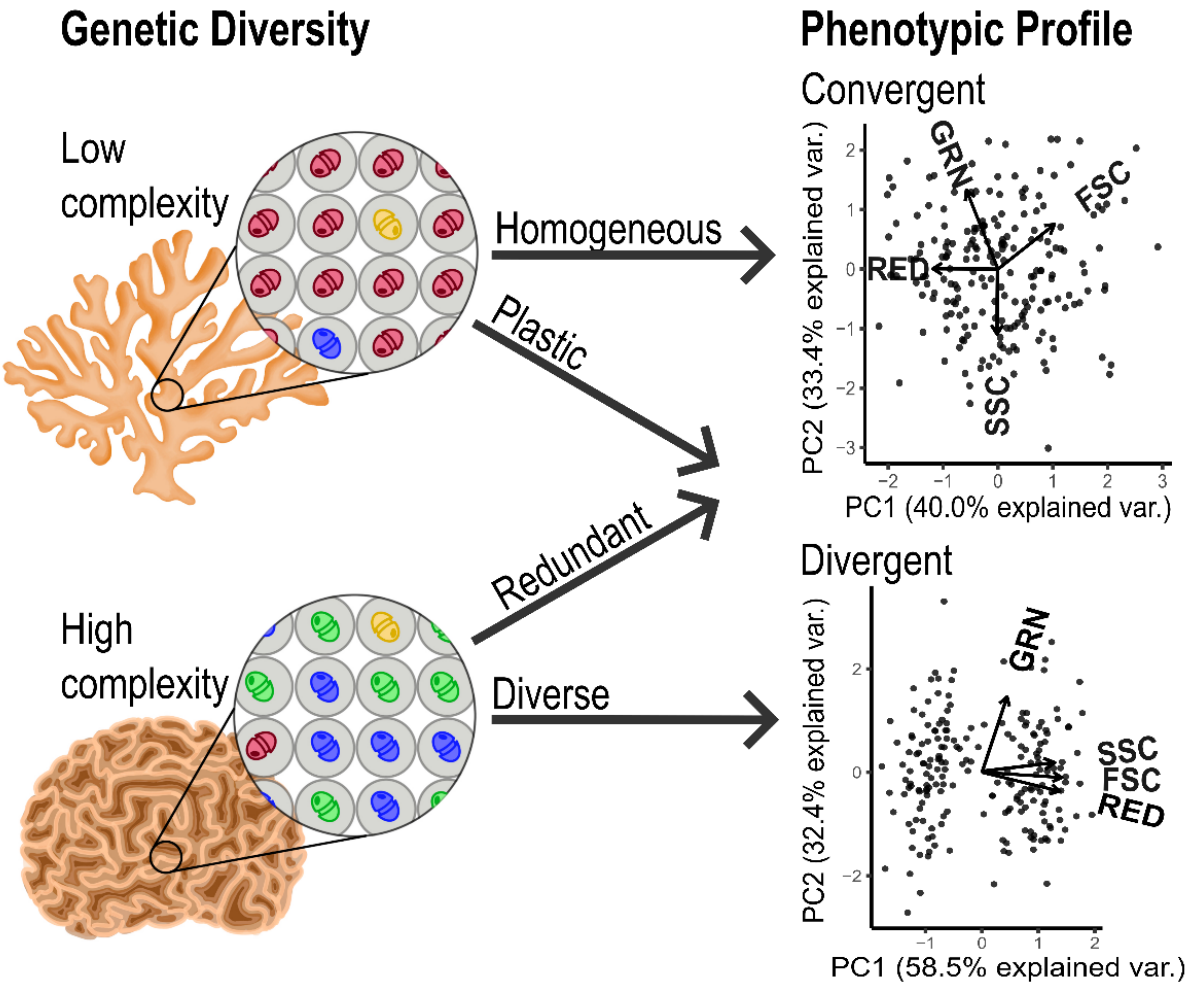

Fig 5: Genetic diversity of Symbiodiniaceae assemblages in-hospite may reveal either low complexity (one dominant clade) or high complexity (more than one dominant clade) communities

[3]; autofluorescence profiles may be either convergent or divergent, as shown here by PCAs consisting of the discussed phenotypic metrics. As indicated by arrows, the combination of genetic diversity and phenotypic profiles has the potential to allow for the classification of Symbiodiniaceae assemblage functional strategies into homogenous, plastic, redundant, or diverse categories upon implementation into other relevant workflows. PCA datasets are theoretical and were generated and analyzed using R.

4.3 Applications. One difficult to answer question is whether changes in physiology of the Symbiodiniaceae assemblages are caused by phenotypic plasticity of individual Symbiodiniaceae cells or shuffling of Symbiodiniaceae assemblages to new functionally advantageous lineages. Integrating our flow cytometry protocol with Symbiodiniaceae metabarcoding would, for example, allow researchers to distinguish between adaptation through symbiont shuffling and acclimation through phenotypic plasticity (Fig 5). Symbiodiniaceae assemblages hosted in corals can either harbor homogeneous Symbiodiniaceae assemblages with low phylogenetic diversity (one dominant genus, species, or strain) or diverse assemblages with high phylogenetic diversity (several codominant genera, species, or strains) [3] (Fig 5). If a coral hosts a highly diverse Symbiodiniaceae assemblage, but the autofluorescence profile detected using our flow cytometry protocol is homogeneous, one may assume functional redundancy of symbiont clades or mediation of Symbiodiniaceae phenotypes by the coral host (Fig 5). Alternatively, if a coral hosts a low diversity Symbiodiniaceae assemblage, but multiple distinct phenotypic profiles are detected, one may assume phenotypic plasticity within the assemblage (Fig 5). Using our protocol for such applications has the potential for providing in-depth understanding of acclimation and adaptation dynamics of corals.

5. Acknowledgements

We would like to thank Rebecca Salas for her assistance running the upside-down jellyfish acclimation experiment and MacKenzie Heagy for illustrating the coral-dinoflagellate assemblages shown in Figure 5.

References

1. LaJeunesse TC, Parkinson JE, Gabrielson PW, Jeong HJ, Reimer JD, Voolstra CR, et al. Systematic revision of Symbiodiniaceae highlights the antiquity and diversity of coral endosymbionts. Curr Biol. 2018;28: 2570–2580.e6. doi:10.1016/j.cub.2018.07.008

2. Hoegh-Guldberg O. Climate change, coral bleaching and the future of the world's coral reefs. Mar Freshwater Res. 1999;50: 839–866. doi:10.1071/mf99078

3. Davies SW, Gamache MH, Howe-Kerr LI, Kriefall NG, Baker AC, Banaszak AT, et al. Building consensus around the assessment and interpretation of Symbiodiniaceae diversity. PeerJ. 2023;11: e15023. doi:10.7717/peerj.15023

4. Warner ME, Fitt WK, Schmidt GW. The effects of elevated temperature on the photosynthetic efficiency of zooxanthellae in hospite from four different species of reef coral: a novel approach. Plant Cell Environ. 1996;19: 291–299. doi:10.1111/j.1365-3040.1996.tb00251.x

5. Suwa R, Hirose M, Hidaka M. Seasonal fluctuation in zooxanthellar genotype composition and photophysiology in the corals *Pavona divaricata* and *P. decussata*. Mar Ecol Prog Ser. 2008;361: 129–137. doi:10.3354/meps07372

6. Berg JT, David CM, Gabriel MM, Bentlage B. Fluorescence signatures of persistent photosystem damage in the staghorn coral *Acropora* cf. *pulchra* (Anthozoa: Scleractinia) during bleaching and recovery. Mar Biol Res. 2020;16: 643–655. doi:10.1080/17451000.2021.1875245

7. Hennige SJ, Suggett DJ, Warner ME, McDougall KE, Smith DJ. Photobiology of Symbiodinium revisited: bio-physical and bio-optical signatures. Coral Reefs. 2009;28: 179–195. doi:10.1007/s00338-008-0444-x

8. Jeong HJ, Lee SY, Kang NS, Yoo YD, Lim AS, Lee MJ, et al. Genetics and morphology characterize the dinoflagellate *Symbiodinium voratum*, n. sp., (Dinophyceae) as the sole representative of Symbiodinium Clade E. J Eukaryot Microbiol. 2014;61: 75–94. doi:10.1111/jeu.12088

9. Mansour JS, Pollock FJ, Díaz-Almeyda E, Iglesias-Prieto R, Medina M. Intra- and interspecific variation and phenotypic plasticity in thylakoid membrane properties across two Symbiodinium clades. Coral Reefs. 2018;37: 841–850. doi:10.1007/s00338-018-1710-1

10. Apprill AM, Bidigare RR, Gates RD. Visibly healthy corals exhibit variable pigment concentrations and symbiont phenotypes. Coral Reefs. 2007;26: 387–397. doi:10.1007/s00338-007-0209-y

11. Lee CS, Yeo YSW, Sin TM. Bleaching response of Symbiodinium (zooxanthellae): determination by flow cytometry. Cytometry A. 2012;81: 888–895. doi:10.1002/cyto.a.22111

12. Muñoz HE, Li M, Riche CT, Nitta N, Diebold E, Lin J, et al. Single-cell analysis of morphological and metabolic heterogeneity in *Euglena gracilis* by fluorescence-imaging flow cytometry. Anal Chem. 2018;90: 11280–11289. doi:10.1021/acs.analchem.8b01794

13. Krediet CJ, DeNofrio JC, Caruso C, Burriesci MS, Cella K, Pringle JR. Rapid, precise, and accurate counts of Symbiodinium cells using the Guava Flow Cytometer, and a comparison

to other methods. PLoS One. 2015;10: e0135725. doi:10.1371/journal.pone.0135725

14. Dittrich WM, Göhde WH. Flow-through chamber for photometers to measure and count particles in a dispersion medium. US Patent. 3761187A, 1973.

15. McKinnon KM. Flow Cytometry: An Overview. Curr Protoc Immunol. 2018;120: 5.1.1–5.1.11. doi:10.1002/cpim.40

16. Yentsch CM, Mague FC, Horan PK, Muirhead K. Flow cytometric DNA determinations on individual cells of the dinoflagellate *Gonyaulax tamarensis* var. *excavata*. J Exp Mar Bio Ecol. 1983;67: 175–183. doi:10.1016/0022-0981(83)90088-6

17. Olson RJ, Frankel SL, Chisholm SW, Shapiro HM. An inexpensive flow cytometer for the analysis of fluorescence signals in phytoplankton: Chlorophyll and DNA distributions. J Exp Mar Bio Ecol. 1983;68: 129–144. doi:10.1016/0022-0981(83)90155-7

18. Lesser MP. Elevated temperatures and ultraviolet radiation cause oxidative stress and inhibit photosynthesis in symbiotic dinoflagellates. Limnol Oceanogr. 1996;41: 271–283. doi:10.4319/lo.1996.41.2.0271

19. Lesser MP. Photobiology of natural populations of zooxanthellae from the sea anemone *Aiptasia pallida*: assessment of the host's role in protection against ultraviolet radiation. Cytometry. 1989;10: 653–658. doi:10.1002/cyto.990100522

20. Dubelaar GBJ, Jonker RR. Flow cytometry as a tool for the study of phytoplankton. Sci Mar. 2000. Available: https://scientiamarina.revistas.csic.es/index.php/scientiamarina/article/view/751

21. Becker A, Meister A, Wilhelm C. Flow cytometric discrimination of various phycobilin-containing phytoplankton groups in a hypertrophic reservoir. Cytometry: The Journal of the. 2002. Available: https://onlinelibrary.wiley.com/doi/abs/10.1002/cyto.10104

22. Freitas C, Parreira TM, Roseiro J, Reis A, da Silva TL. Selecting low-cost carbon sources for carotenoid and lipid production by the pink yeast *Rhodosporidium toruloides* NCYC 921 using flow cytometry. Bioresour Technol. 2014;158: 355–359. doi:10.1016/j.biortech.2014.02.071

23. Ukibe K, Katsuragi T, Tani Y, Takagi H. Efficient screening for astaxanthin-overproducing mutants of the yeast *Xanthophyllomyces dendrorhous* by flow cytometry. FEMS Microbiol Lett. 2008;286: 241–248. doi:10.1111/j.1574-6968.2008.01278.x

24. McIlroy SE, Smith GJ, Geller JB. FISH-Flow: a quantitative molecular approach for describing mixed clade communities of Symbiodinium. Coral Reefs. 2014;33: 157–167. doi:10.1007/s00338-013-1087-0

25. Patten NL, Seymour JR, Mitchell JG. Flow cytometric analysis of virus-like particles and heterotrophic bacteria within coral-associated reef water. J Mar Biol Assoc U K. 2006;86: 563–566. doi:10.1017/S0025315406013476

26. Bettarel Y, Thanh MC, Patrice G, Antoinette A, Nadège K-N, Bui VN, et al. Flow cytometric enumeration of bacterial in the coral surface mucus layer. J Microbiol Methods. 2016;128: 16–19. doi:10.1016/j.mimet.2016.05.032

27. Fujise L, Nitschke MR, Frommlet JC, Serôdio J, Woodcock S, Ralph PJ, et al. Cell cycle dynamics of cultured coral endosymbiotic microalgae (Symbiodinium) across different

types (species) under alternate light and temperature conditions. J Eukaryot Microbiol. 2018;65: 505–517. doi:10.1111/jeu.12497

28. Tivey TR, Parkinson JE, Weis VM. Host and Symbiont Cell Cycle Coordination Is Mediated by Symbiotic State, Nutrition, and Partner Identity in a Model Cnidarian-Dinoflagellate Symbiosis. MBio. 2020;11. doi:10.1128/mBio.02626-19

29. Figueroa RI, Howe-Kerr LI, Correa AMS. Direct evidence of sex and a hypothesis about meiosis in Symbiodiniaceae. Sci Rep. 2021;11: 18838. doi:10.1038/s41598-021-98148-9

30. Mukherjee A, Walker J, Weyant KB, Schroeder CM. Characterization of flavin-based fluorescent proteins: an emerging class of fluorescent reporters. PLoS One. 2013;8: e64753. doi:10.1371/journal.pone.0064753

31. Venn AA, Wilson MA, Trapido-Rosenthal HG, Keely BJ, Douglas AE. The impact of coral bleaching on the pigment profile of the symbiotic alga, Symbiodinium. Plant Cell Environ. 2006;29: 2133–2142. doi:10.1111/j.1365-3040.2006.001587.x

32. Koziol AG, Borza T, Ishida K-I, Keeling P, Lee RW, Durnford DG. Tracing the evolution of the light-harvesting antennae in chlorophyll a/b-containing organisms. Plant Physiol. 2007;143: 1802–1816. doi:10.1104/pp.106.092536

33. Zapata M, Edvardsen B, Rodríguez F, Maestro MA, Garrido JL. Chlorophyll c2 monogalactosyldiacylglyceride ester (chl c2-MGDG). A novel marker pigment for Chrysochromulina species (Haptophyta). Mar Ecol Prog Ser. 2001;219: 85–98. doi:10.3354/meps219085

34. Koyama Y, Hashimoto H. Spectroscopic studies of carotenoids in photosynthetic systems. In: Young AJ, Britton G, editors. Carotenoids in Photosynthesis. Dordrecht: Springer Netherlands; 1993. pp. 327–408. doi:10.1007/978-94-011-2124-8_9

35. Jiang J, Zhang H, Kang Y, Bina D, Lo CS, Blankenship RE. Characterization of the peridinin–chlorophyll a-protein complex in the dinoflagellate Symbiodinium. Biochimica et Biophysica Acta (BBA) - Bioenergetics. 2012;1817: 983–989. doi:10.1016/j.bbabio.2012.03.027

36. Yacobi YZ. Review: From Tswett to identified flying objects: A concise history of chlorophyll a use for quantification of phytoplankton. Isr J Plant Sci. 2012;60: 243–251. doi:10.1560/IJPS.60.1-2.243

37. Kagatani K, Nagao R, Shen J-R, Yamano Y, Takaichi S, Akimoto S. Excitation relaxation dynamics of carotenoids constituting the diadinoxanthin cycle. Photosynth Res. 2022;154: 13–19. doi:10.1007/s11120-022-00944-5

38. Niedzwiedzki DM, Magdaong NCM, Su X. Biochemical and spectroscopic characterizations of the oligomeric antenna of the coral symbiotic Symbiodiniaceae *Fugacium kawagutii*. Photosynth Res. 2022. Available: https://link.springer.com/article/10.1007/s11120-022-00951-6

39. Koziol B, Markowicz M, Kruk J, Plytycz B. Riboflavin as a source of autofluorescence in *Eisenia fetida* coelomocytes. Photochem Photobiol. 2006;82: 570–573. doi:10.1562/2005-11-23-RA-738

40. Fujita S, Iseki M, Yoshikawa S, Makino Y, Watanabe M, Motomura T, et al. Identification

and characterization of a fluorescent flagellar protein from the brown alga *Scytosiphon lomentaria* (Scytosiphonales, Phaeophyceae): A flavoprotein homologous to Old Yellow Enzyme. Eur J Phycol. 2005;40: 159–167. doi:10.1080/09670260500063193

41. Bricaud A. Natural variability of phytoplanktonic absorption in oceanic waters: Influence of the size structure of algal populations. J Geophys Res. 2004;109. doi:10.1029/2004jc002419

42. Schoefs B. Chlorophyll and carotenoid analysis in food products. Properties of the pigments and methods of analysis. Trends Food Sci Technol. 2002;13: 361–371. doi:10.1016/S0924-2244(02)00182-6

43. Mullaney PF, Van Dilla MA, Coulter JR, Dean PN. Cell sizing: a light scattering photometer for rapid volume determination. Rev Sci Instrum. 1969;40: 1029–1032. doi:10.1063/1.1684143

44. Steen HB. Further developments of a microscope-based flow cytometer: light scatter detection and excitation intensity compensation. Cytometry. 1980;1: 26–31. doi:10.1002/cyto.990010107

45. Jaso JM. Introduction to flow cytometry. 1991. Available: http://www.hemepathreview.com/Heme-Review/FlowCytometry.pdf

46. Shapiro HM. Practical Flow Cytometry. John Wiley & Sons; 2005. Available: https://play.google.com/store/books/details?id=JhSyimPKuJwC

47. Ogle DH, Doll JC, Wheeler P, Dinno A. FSA. Fisheries Stock Analysis R Package Version.

48. Mangiafico S. rcompanion: Functions to Support Extension Education Program Evaluation.

2023. Available: https://CRAN.R-project.org/package=rcompanion

49. Medina M, Sharp V, Ohdera AH, Bellantuono A, Dalrymple J, Gamero-Mora E, et al. The upside-down jellyfish *Cassiopea xamachana* as an emerging model system to study cnidarian--algal symbiosis. Handbook of marine model organisms in experimental biology established and emerging Edited By. 2021. Available: https://repositorio.usp.br/bitstreams/fc73e2aa-2fca-4a4a-a593-f85002a70b6f

50. Anthony CJ, Heagy M, Bentlage B. Phenotypic plasticity in *Cassiopea ornata* (Cnidaria: Scyphozoa: Rhizostomeae) suggests environmentally driven morphology. Zoomorphology. 2022;141: 115–131. doi:10.1007/s00435-022-00558-4

51. Bunn A, Korpela M. Crossdating in dplR. [cited 18 May 2023]. Available: https://cran.microsoft.com/snapshot/2014-09-08/web/packages/dplR/vignettes/xdate-dplR.pdf

52. Team RS. RStudio: integrated development for R. (No Title). 2015 [cited 18 May 2023]. Available: https://cir.nii.ac.jp/crid/1370004240607707919

53. Wickham H. ggplot2: Elegant Graphics for Data Analysis. Springer; 2016. Available: https://play.google.com/store/books/details?id=XgFkDAAAQBAJ

54. Polívka T, Hiller RG, Frank HA. Spectroscopy of the peridinin–chlorophyll-a protein: Insight into light-harvesting strategy of marine algae. Arch Biochem Biophys. 2007;458: 111–120. doi:10.1016/j.abb.2006.10.006

55. Kato H, Tokutsu R, Kubota-Kawai H, Burton-Smith RN, Kim E, Minagawa J.

Characterization of a Giant PSI Supercomplex in the Symbiotic Dinoflagellate Symbiodiniaceae. Plant Physiol. 2020;183: 1725–1734. doi:10.1104/pp.20.00726

56. Frank HA, Cua A, Chynwat V, Young A, Gosztola D, Wasielewski MR. The lifetimes and energies of the first excited singlet states of diadinoxanthin and diatoxanthin: the role of these molecules in excess energy dissipation in algae. Biochimica et Biophysica Acta (BBA) - Bioenergetics. 1996;1277: 243–252. doi:10.1016/S0005-2728(96)00106-5

57. Olson RJ, Zettler ER, Anderson OK. Discrimination of eukaryotic phytoplankton cell types from light scatter and autofluorescence properties measured by flow cytometry. Cytometry. 1989;10: 636–643. doi:10.1002/cyto.990100520

58. Premazzi G, Buonaccorsi G, Zilio P. Flow cytometry for algal studies. Water Res. 1989;23: 431–442. doi:10.1016/0043-1354(89)90134-6

59. Hiller RG, Wrench PM, Gooley AP, Shoebridge G, Breton J. The major intrinsic light-harvesting protein of Amphidinium: characterization and relation to other light-harvesting proteins. Photochem Photobiol. 1993;57: 125–131. doi:10.1111/j.1751-1097.1993.tb02267.x

60. Niedzwiedzki DM, Jiang J, Lo CS, Blankenship RE. Spectroscopic properties of the Chlorophyll a-Chlorophyll c 2-Peridinin-Protein-Complex (acpPC) from the coral symbiotic dinoflagellate Symbiodinium. Photosynth Res. 2014;120: 125–139. doi:10.1007/s11120-013-9794-5

61. Cooper ED, Bentlage B, Gibbons TR, Bachvaroff TR, Delwiche CF. Metatranscriptome profiling of a harmful algal bloom. Harmful Algae. 2014;37: 75–83.

doi:10.1016/j.hal.2014.04.016

62. Kanazawa A, Blanchard GJ, Szabó M, Ralph PJ, Kramer DM. The site of regulation of light capture in Symbiodinium: Does the peridinin–chlorophyll a–protein detach to regulate light capture? Biochimica et Biophysica Acta (BBA) - Bioenergetics. 2014;1837: 1227–1234. doi:10.1016/j.bbabio.2014.03.019

63. Schulte T, Johanning S, Hofmann E. Structure and function of native and refolded peridinin-chlorophyll-proteins from dinoflagellates. Eur J Cell Biol. 2010;89: 990–997. doi:10.1016/j.ejcb.2010.08.004

64. Takahashi S, Whitney S, Itoh S, Maruyama T, Badger M. Heat stress causes inhibition of the de novo synthesis of antenna proteins and photobleaching in cultured Symbiodinium. Proc Natl Acad Sci U S A. 2008;105: 4203–4208. doi:10.1073/pnas.0708554105

65. Cutzu R, Clemente A, Reis A, Nobre B, Mannazzu I, Roseiro J, et al. Assessment of β-carotene content, cell physiology and morphology of the yellow yeast *Rhodotorula glutinis* mutant 400A15 using flow cytometry. J Ind Microbiol Biotechnol. 2013;40: 865–875. doi:10.1007/s10295-013-1278-2

66. Stahl W, Sies H. Antioxidant activity of carotenoids. Mol Aspects Med. 2003;24: 345–351. doi:10.1016/s0098-2997(03)00030-x

67. Burton GW. Antioxidant action of carotenoids. J Nutr. 1989;119: 109–111. doi:10.1093/jn/119.1.109

68. Young A, Britton G. Carotenoids in Photosynthesis. Springer Netherlands; 2012. Available:

https://play.google.com/store/books/details?id=UrlfmQEACAAJ

69. Smerilli A, Orefice I, Corato F, Gavalás Olea A, Ruban AV, Brunet C. Photoprotective and antioxidant responses to light spectrum and intensity variations in the coastal diatom *Skeletonema marinoi*. Environ Microbiol. 2017;19: 611–627. doi:10.1111/1462-2920.13545

70. D'Amico-Damião V, Carvalho RF. Cryptochrome-Related Abiotic Stress Responses in Plants. Front Plant Sci. 2018;9: 1897. doi:10.3389/fpls.2018.01897

71. Yu X, Liu H, Klejnot J, Lin C. The Cryptochrome Blue Light Receptors. Arabidopsis Book. 2010;8: e0135. doi:10.1199/tab.0135

72. Deng B, Jin X, Yang Y, Lin Z, Zhang Y. The regulatory role of riboflavin in the drought tolerance of tobacco plants depends on ROS production. Plant Growth Regul. 2014;72: 269–277. doi:10.1007/s10725-013-9858-8

73. Taheri P, Tarighi S. Riboflavin induces resistance in rice against *Rhizoctonia solani* via jasmonate-mediated priming of phenylpropanoid pathway. J Plant Physiol. 2010;167: 201–208. doi:10.1016/j.jplph.2009.08.003

74. Sandoval FJ, Zhang Y, Roje S. Flavin nucleotide metabolism in plants: monofunctional enzymes synthesize fad in plastids. J Biol Chem. 2008;283: 30890–30900. doi:10.1074/jbc.M803416200

75. Tzur A, Moore JK, Jorgensen P, Shapiro HM. Optimizing optical flow cytometry for cell volume-based sorting and analysis. PLoS One. 2011. Available: https://journals.plos.org/plosone/article?id=10.1371/journal.pone.0016053

76. Anthony CJ, Lock C, Taylor BM, Bentlage B. Photosystem regulation in coral-associated dinoflagellates (Symbiodiniaceae) is the primary mode for seasonal acclimation. bioRxiv. 2022. p. 2022.12.24.520888. doi:10.1101/2022.12.24.520888

77. Thornhill DJ, Daniel MW, LaJeunesse TC, Schmidt GW, Fitt WK. Natural infections of aposymbiotic *Cassiopea xamachana* scyphistomae from environmental pools of Symbiodinium. J Exp Mar Bio Ecol. 2006;338: 50–56. doi:10.1016/j.jembe.2006.06.032

Supporting information

S1 File. Protocol to quantify photophysiology of endosymbiotic dinoflagellates using the Guava Flow Cytometer. Also available on protocols.io: https://www.protocols.io/private/4DD4507110B911EE9A3E0A58A9FEAC02 (doi will be released prior to publication).